Thermal stratification effects on turbulence and dispersion in internal and external boundary layers

Vincenzo Sessa[a], Zheng-Tong Xie[a,*], Steven Herring[b]

[a] *University of Southampton, Southampton, SO17 1BJ, UK*
[b] *Dstl, Porton Down, Salisbury, SP4 0JQ, UK*

Abstract

A synthetic turbulence and temperature fluctuation generation method embedded in large–eddy simulations (LES) was developed to investigate the effects of weakly stable stratification (i.e. with the Richardson number $R_i \leq 1$) on turbulence and dispersion following a rural–to–urban transition region. The work was based on firstly validating predictions of mean velocity, turbulent stresses and point–source dispersion against wind tunnel experiments of a stable boundary layer approaching a regular array of uniform cuboid elements at $R_i = 0.21$. The depth of the internal boundary layer (IBL) formed at the leading edge of the uniform array was determined using the method which we have previously proposed. Vertical profiles of wall–normal turbulent stress showed that the height and the growth rate of the IBL were sensitive to the thermal stability prescribed at the inlet. We found that the IBL height was reduced when the inflow turbulent kinetic energy (TKE) was reduced while maintaining the same stratification condition. Lastly, scalar fluxes and mean concentrations within and above the canopy from a ground–level line source were simulated and analysed. It was found that increasing the stable stratification level reduced the vertical transport of pollutant which increased the volume–averaged concentration within the canopy. For a given level of stable stratification, the effect on the total scalar fluxes within and above the canopy, and on the volume-averaged mean

*Corresponding author
Email address: Z.Xie@soton.ac.uk (Zheng-Tong Xie)

concentration within the lateral streets is more pronounced when the TKE is reduced.

Keywords: IBL, inflow turbulence, stable stratification, dispersion

1. Introduction

Nearly two decays ago Britter & Hanna (2003) suggested that urban flows may be considered as neutral or nearly neutral in urban dispersion models. However, the topic of thermal stratification in urban area has recently renewed attention (e.g. Kanda & Yamao, 2016; Boppana et al., 2013), from which it has been concluded that non–neutral atmospheric stratification conditions frequently occur in urban areas and neutral conditions may be the exception rather than the rule (Wood et al., 2010). It has been documented that unstable thermal conditions occur three times more frequently than stable and six times more than neutral conditions over the city of London during the daytime. Furthermore, at night the number of unstable cases was almost equal to the number of stable cases and four times greater than the number of neutral ones, because of radiative cooling of the surface.

In stable conditions pollutant concentration may increase and air quality may decrease within urban canopy because of the reduced dispersion in vertical direction. Despite the increasing concerns regarding air quality, only a few experimental studies have examined the effects of stable stratification on turbulent structures over smooth, rough (e.g. Ohya, 2001; Williams et al., 2017), and very rough to urban (e.g. Marucci & Carpentieri, 2018a; Marucci et al., 2018b) surfaces, and the impact on passive scalar dispersion (e.g. Yassin et al., 2005; Kanda & Yamao, 2016). Not surprisingly, only a very few numerical studies (e.g. Cheng & Liu, 2011; Xie et al., 2013; Boppana et al., 2013; Tomas et al., 2016) have examined turbulence and dispersion in stably stratified flows over very rough – urban surfaces. Two key problems remain to be addressed.

The first problem is to identify the critical level of stratification which can be interpreted as signalling the start of 'strongly' stratified region. Williams

et al. (2017) reported that the critical bulk Richardson number, based on the boundary layer thickness, the free stream velocity and the temperature difference across the boundary layer thickness, was 0.10 for a smooth surface, while the critical bulk Richardson number was 0.15 for a rough surface with roughness length in wall units z_0^+ less than 4. This confirms that a rough surface reduces stratification effect compared to smooth wall, and also suggests that for a very rough urban surface, which would have a much greater roughness length, the critical Richardson number is likely to be greater than 0.15.

The second problem is that the urban surface is always heterogeneous. The change in surface roughness associated with a flow crossing from a rural area into an urban area, or low-rise buildings area into a central business district (CBD) with high-rise buildings, leads to a region of transitional flow as the turbulent boundary adapts to the new wall condition (e.g. Hanson & Ganapathisubramani, 2016; Cheng & Castro, 2002; Tomas et al., 2016; Marucci et al., 2018b; Sessa et al., 2018). This transitional flow results from the development of an internal boundary layer (IBL) above the roughness elements. To understand how air quality may be impacted, it is necessary to determine to what extent that the step change of roughness and the thermal stratification together affect flow and dispersion.

Tomas et al. (2016) investigated the effect of stable stratification on flow and line source dispersion by simulating a smooth–wall boundary layer entering a generic urban area using large-eddy simulation (LES). Although they only considered a weakly stable condition with a bulk Richardson number of 0.147, they found that the IBL was 14% shallower than that in neutral conditions and the turbulent kinetic energy (TKE) was reduced by 21%. It should be noted that the approaching flow was developed over a smooth–wall surface so that the inflow turbulence intensity and integral length scales were not representative of a typical rural boundary layer. This means that the subsequent turbulence and dispersion predictions downstream of the step change in surface roughness are not representative of a true rural-urban surface.

The effects of stable stratification on turbulence and dispersion are not neg-

ligible even under weakly stable conditions (e.g. Xie et al., 2013; Boppana et al., 2014). The consumption of buoyancy energy in such conditions damps turbulence which affects ventilation and the concentration of pollutants at pedestrian level. When Cheng & Liu (2011) investigated stability effects at bulk Richardson numbers of 0.18 and 0.35 on the dispersion in $2D$ street canyons using LES, they found that for a Richardson number greater than 0.25, turbulence was strongly suppressed at ground level. This meant that the pollutant tended to reside longer at pedestrian level than in the upper street canyon. Tomas et al. (2016) showed that for a bulk Richardson number of 0.147 the area–averaged street concentration of a line source was 17% higher than in neutral conditions due to decreased streamwise advection and trapping of pollutant by the IBL. Similar conclusions were reached in the LES study conducted by Xie et al. (2013), who found that the stability effects induced at a bulk Richardson number of 0.21 increased mean concentrations by up to an order of magnitude when compared to neutral conditions. Moreover, Xie et al. (2013) also found that turbulent fluctuations and mean velocities were not substantially affected either by a change of mean temperature profile below the canopy or inlet temperature fluctuations for a given Richardson number.

As far as we are aware, very few studies have examined the effects of stable stratification on dispersion within an IBL, and those that have have only considered weakly stable conditions. In this paper we consider the effects of various stratification conditions up to a bulk Richardson number 1.0 on turbulence and dispersion following a rural–to–urban transition. The objective was to use LES to answer the following three questions:

1. To what extent are stratification effects on flow and dispersion following a step change in roughness length dependent on the inflow turbulence intensity?

2. To what extent extent does increasing stratification affect the IBL thickness for bulk R_i numbers below 1?

3. To what extent does increasing stratification affect the ventilation of pollutant within and above the canopy for bulk R_i numbers below 1?

The governing equations are briefly described in Sect. 2. Details of numeri-

cal settings including geometry, mesh and inflow conditions are given in Sect. 3. LES validation, sensitivity tests on the ground temperature and turbulent kinetic energy at inlet are reported in Sect. 4.1. Stratification effects on the internal boundary layer are discussed in Sect. 5. The analysis of scalar fluxes and mean concentration results are reported in Sect. 6. Finally, the conclusions are summarised in Sect. 7.

2. Governing equations

In LES the filtered continuity and momentum equations for a buoyancy–driven flow are written as follows:

$$\frac{\partial u_i}{\partial x_i} = 0 \tag{1}$$

$$\frac{\partial u_i}{\partial t} + \frac{\partial u_i u_j}{\partial x_j} = -\frac{1}{\rho}\frac{\partial p}{\partial x_i} + f\delta_{i2} + \frac{\partial}{\partial x_j}\left(\frac{\tau_{ij}}{\rho} + \nu\frac{\partial u_i}{\partial x_j}\right) \tag{2}$$

where the filtered velocity and pressure fields are u_i and p respectively, ν is the kinematic molecular viscosity and ρ is the density. τ_{ij} is the subgrid–scale (SGS) Reynolds stress which was determined by using the mixed time–scale subgrid eddy viscosity model (Inagaki et al., 2005). $f\delta_{i2}$ is the body force due to thermal buoyancy and is calculated by using the Boussinesq approximation.

The filtered transport equation for a passive scalar is:

$$\frac{\partial C}{\partial t} + \frac{\partial u_j C}{\partial x_j} = \frac{\partial}{\partial x_j}\left[(K + K_r)\frac{\partial C}{\partial x_j}\right] + S \tag{3}$$

where C is the filtered scalar concentration and S is a source term. The second term on the left–hand side is the advection term and the first term on the right–hand side is the diffusion term. K is the molecular diffusivity and K_r is the subgrid-scale (SGS) turbulent diffusivity computed as:

$$K_r = \frac{\nu_r}{Sc_r} \tag{4}$$

where ν_r is the SGS viscosity and Sc_r is the subgrid Schmidt number. A constant Schmidt number of $Sc_r = 0.7$ was assumed.

The filtered transport equation of temperature is:

$$\frac{\partial T}{\partial t} + \frac{\partial u_j T}{\partial x_j} = \frac{\partial}{\partial x_j}\left[(D + D_r)\frac{\partial T}{\partial x_j}\right] \tag{5}$$

where T is the resolved–scale temperature. D is the molecular diffusivity of temperature, D_r is the subgrid turbulent diffusivity and is given by ν_r/Pr_r, where Pr_r is the subgrid Prandtl number was set to 0.9.

3. Numerical settings

The LES model was implemented within the open-source CFD package OpenFOAM version 2.1.1. A second-order backward implicit scheme in time and second–order central difference scheme in space were applied for the discretisation of the terms in Eqs. 2, 3 and 5. The domain was set as a half channel. An efficient inflow turbulence generation method (Xie & Castro, 2008) was used at the inlet, with periodic conditions at the lateral boundaries and a stress–free condition at the top of the domain ($y = 12h$, where $h = 70mm$ was the uniform height of the array element). The Reynolds number based on h and the free stream velocity $u_{ref} = 1.35m/s$ at $y = 12h$ was approximately $8,000$. The average CFL number was 0.2, based on a time step resolution of $0.0007s$. Flow and second-order statistics were initialized for 20 flow-passes and then averaged over 150 flow–passes.

For purpos of validating the baseline study, numerical settings, e.g. the geometry of the array, the point source, the approaching boundary layer and the thermal stratification conditions, were made as consistent as possible with experiments conducted by, i.e. Castro et al. (2017), Hertwig et al. (2018), Marucci et al. (2018b) and Marucci & Carpentieri (2018a). The wind tunnel experiments were conducted using the meterological wind tunnel at the University of Surrey, UK, which has a test section 20m (length) x 3.5m (width) x1.5m (height). The wind tunnel is able to generate a 'simulated' atmospheric boundary layer representative of stable and unstable conditions by using Irwin's spires, two-dimensional roughness elements and adjusting the inlet and floor temperature.

Propane was used as a passive tracer and its concentration was meausred by using a fast flame ionisation detector system (FFID). Velocites were measured by using a two-component laser-Doppler anemometry (LDA). Mean temperature and its fluctuations were measured using a fast-response cold-wire probe (CW). More generic details can be found in the above references. The numerical settings applied to simulate the flow and point source dispersion in neutral conditions were consistent with those in Castro et al. (2017) and Hertwig et al. (2018), respectively. For the studies in stable conditions, the numerical settings applied to the flow and point source dispersion were consistent with those in Marucci et al. (2018b) and Marucci & Carpentieri (2018a), respectively. More specific details are given in the following sections.

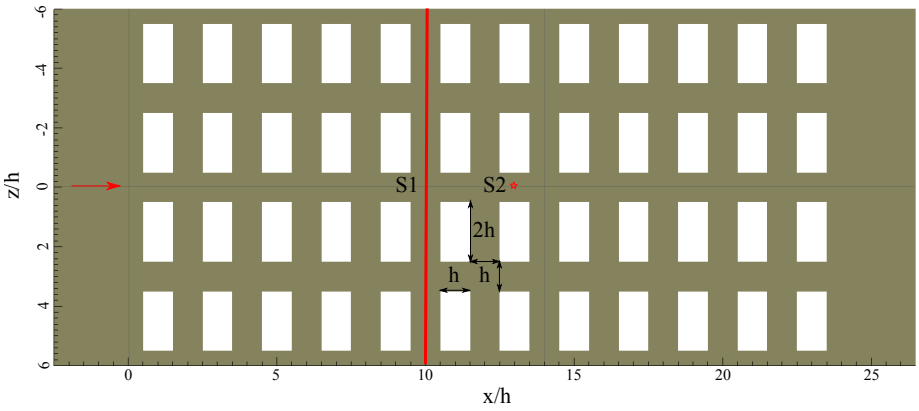

Figure 1: Plan view of the array configuration showing dimensions of buildings and streets, coordinate system, flow direction, and locations of line source $S1$ and point source $S2$.

3.1. Geometry, mesh and resolution

The array of regular cuboid elements modelled in this paper represents part of a larger array used in the wind tunnel experiments of Castro et al. (2017) and Marucci et al. (2018b). This array was designed to simulate a neighbourhood scale region in which statistical homogeneities are assumed. The basic obstacle layout is identical to those described in Sessa et al. (2018) and in Fuka et al. (2017).

A plan view of the modelled array is shown in Fig. 1 where the street units parallel to the x axis are $1h$ long and referred to as 'short streets' hereinafter. Street units parallel to the z axis are $2h$ long and referred to as 'long streets'. The rectangular array comprised 48 aligned blocks with h spacing, which leads to a plan area density of $\lambda_p = 0.33$ when considering the single block unit.

The dimensions of the modelled domain were $31.5h \times 12h \times 12h$ within a uniform Cartesian grid of resolution $\triangle = h/16$. The top boundary was placed at $y = 12h$ to be very close to the experimental boundary layer height (Marucci et al., 2018b). In order to ensure the zero–gradient outflow boundary condition, the domain size was extended by $2.5h$ in x–direction compared to the domain used in Sessa et al. (2018). Computations were made for the 0° wind direction by assuming that the mean wind flow was perpendicular to the front face of the cuboid elements as indicated in Fig. 1.

3.2. Scalar sources

A passive scalar was released from a ground–level point source (S2) and a ground–level line source (S1) within the array of cuboid elements. Because of the finite size of the grid, the shape of the point source only approximated the source used in the experiment. The shape and size of the point source was identical to that reported in Fuka et al. (2017). The diameter was represented by 4 cells and so measured $0.25h$, while the height was one cell ($h/16$). The point source was positioned in the middle of a short street within the seventh row of blocks (Fig. 1) in accordance with the experimental set–up of Marucci et al. (2018b).

The line source was positioned on the ground between the fifth and sixth rows of blocks. The lateral extent of the line source was set equal to the entire width of the domain ($12h$) while the height and width of it were one cell ($h/16$) and four cells ($4h/16$) respectively. A constant scalar flux release rate was set for each cell inside the volume of both the point source and the line source.

3.3. Inlet conditions of temperature for LES

In order to analyse the effects of thermal stratification on flow and dispersion, LES simulations were conducted for various bulk Richardson numbers R_i, defined as:

$$R_i = \frac{gH(\overline{T}_{ref} - \overline{T}_0)}{\overline{T}_0 \overline{u}^2_{ref}} \tag{6}$$

where $\overline{u}_{ref}$ is the freestream velocity at the inlet, g is the acceleration due to gravity, H is the domain height and $\overline{T}_0$ is the mean temperature on the ground. LES comparisons for increasing stable stratification were achieved in a similar manner to Boppana et al. (2013), by fixing $\overline{T}_{ref}$ and $\overline{T}_0$ and changing the value of g as shown in Tab. 1. The upstream boundary layer height was kept fixed at $H = 12h$ in the LES simulations for all values of R_i, as in the wind tunnel experiments of Marucci et al. (2018b) in which the tendency towards reducing boundary layer height with increasing stability was overcome by the level of turbulence generated by the inlet spires.

The LES requires a continuous specification of turbulence in time at the inlet to simulate an evolving turbulent boundary layer. This was achieved by using the inflow turbulence method developed by Xie & Castro (2008) to generate a synthetic turbulent inflow with exponential–form correlations in time and space. This inflow method has been shown to provide a high fidelity reconstruction of the turbulence characteristics in both the energy–containing region and inertial sublayer of the spectra. Moreover, recent work by Bercin et al. (2018) has shown that that the exponential form correlations provide a better approx than the Gaussian ones.

Table 1: LES variation of gravity g with R_i

Case	R_i	g
R_i=0	0.00	9.81
R_i=0.21	0.21	0.74
R_i=0.5	0.50	1.77
R_i=0.7	0.70	2.48
R_i=1	1.00	3.54
$R_i = 1^*$	1.00	3.54

Figure 2: Vertical profiles of prescribed integral length scales at the LES inlet $x = -2.5h$.

The turbulence generated by the inflow method satisfies the prescribed integral length scales and Reynolds stress-tensor values. The integral length scales L_x, L_y and L_z prescribed in the streamwise, vertical and lateral directions respectively are shown in Fig. 2. These were estimated from data presented in Marucci et al. (2018b) for an experiment simulating $R_i = 0.21$.

The estimated integral length scales can have considerable uncertainties due to the complexity of auto-correlation function, etc. Xie & Castro (2008) performed numerical sensitivity tests using different length scale combinations imposed at inlet (i.e. L_x, L_y and L_z factored by 0.5, 1 or 2). They found that the mean velocities and turbulent stresses within or immediately above the canopy were not sensitive to these variations provided the baseline length scales are not too different from the 'true' values. This suggested that it was not necessary to consider the effect of integral length scales in the current work.

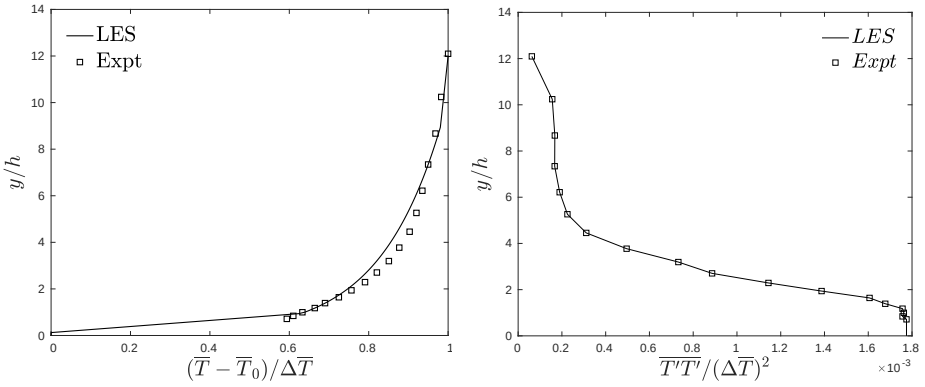

Figure 3: (a) Vertical profiles of laterally averaged mean temperature from LES at inlet and prescribed mean temperature from experiments. (b) Vertical profiles of prescribed temperature variance at the LES inlet and experimental values.

The inflow turbulence method of Xie & Castro (2008) was also used to generate temperature fluctuations. The integral length scale of turbulence in the vertical direction L_y (Fig. 2) was chosen as the integral length scale of temperature fluctuations. Xie et al. (2013) and Okaze & Mochida (2017) used similar approaches to generate flow temperature fluctuations, whereas Xie et al. (2013) did not carried out a validation and Okaze & Mochida (2017) considered temperature as passive scalar. The prescribed mean temperature (Fig. 3a) and temperature variance (Fig. 3b) were obtained from the wind tunnel experiment at $R_i = 0.21$ reported in Marucci et al. (2018b) by assuming lateral homogeneity. Marucci et al. (2018b) fitted the mean temperature profile (Fig. 3a) for $R_i = 0.21$ in the usual log–law form,

$$T(y) - T_0 = \frac{T_*}{\kappa}\left[\ln(\frac{y-d}{y_{0h}}) + 16\frac{y-d-y_{0h}}{L}\right], \tag{7}$$

where the von-Karman constant $\kappa = 0.41$, the roughness displacement height $d = 0$, the ratio of the boundary layer thickness to the Monin-Obukhov length H/L=1.13, the scaling temperature $T_* = 0.34K$, the thermal roughness length $y_{0h} = 0.021mm$, and the maximum temperature difference $\Delta\overline{T}_{MAX}$ between the cooled floor $\overline{T}_0$ and the free stream flow $\overline{T}_{ref}$ was fixed as $16K$. Because

of the experimental uncertainty in measuring temperature values close to the ground, Marucci et al. (2018b) applied the least–squares fitting procedure to estimate the ground temperature $\overline{T_0}$ shown in Hancock & Hayden (2018).

Figure 3b shows the prescribed temperature variance at the LES inlet and the experimental values. A constant temperature variance was prescribed in the vicinity of the floor ($h \leq 1$) where we assume there is a surface layer. The flow within the array of cuboid elements was assumed to be adiabatic, as the inlet wind speed was high, the air pass-through time over the array was short, and the local heat transfer over the block surfaces was negligible. This assumption was validated against data from the wind tunnel experiments of Marucci & Carpentieri (2018a) in Sec. 4.1.

3.4. Inlet conditions of velocities for LES

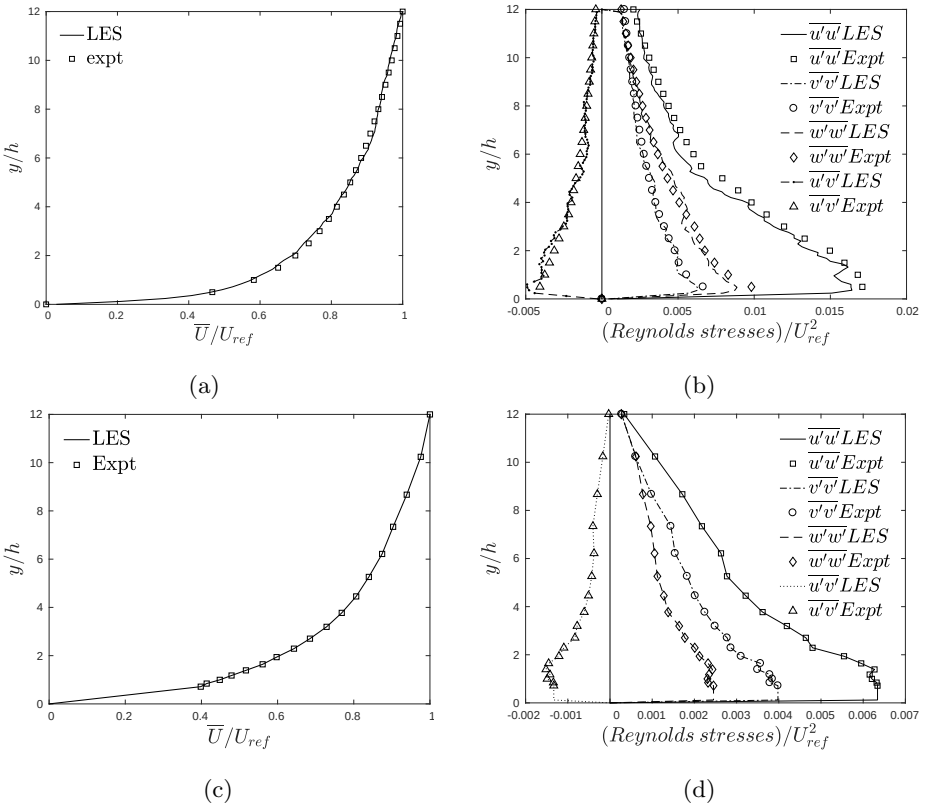

Figure 4: Vertical profiles of experimental and numerically prescribed inlet mean velocity and turbulent stresses. (a) mean velocity,$R_i = 0$; (b) turbulent stresses, $R_i = 0$; (c) mean velocity, $R_i = 0.21$; (d) turbulent stresses, $R_i = 0.21$.

Figure 4a and Fig. 4b show vertical profiles of experimental data (Marucci et al., 2018b) and numerically (Sessa et al., 2018) prescribed inlet mean velocity and turbulent stresses in neutral condition $R_i = 0$, respectively. Figure 4c and Fig. 4d show vertical profiles of experimental data (Marucci et al., 2018b) and numerically prescribed inlet mean velocity and turbulent stresses respectively, at $R_i = 0.21$. The prescribed inlet mean velocity and turbulent stresses for the cases $R_i = 0.5, 0.7, 1$ (Table 1) were the same as those for the case $R_i = 0.21$. This was useful for quantifying to which extent the thermal stratification alone

impacted turbulence and dispersion, as in Xie et al. (2013).

The case $R_i = 1^*$ (Table 1) was designed to quantify the effect of inlet TKE. The inlet mean velocity profile was prescribed to be the same as that of $R_i = 1$, while the turbulent stresses were estimated using a simple method. The ratios of the friction velocity to the freestream velocity u_*/u_{ref} at $R_i = 0, 0.14, 0.21, 0.33$ reported in Marucci et al. (2018b) were normalised by that at $R_i = 0.21$, and fitted to an exponential–function of R_i number(Fig. 5a).

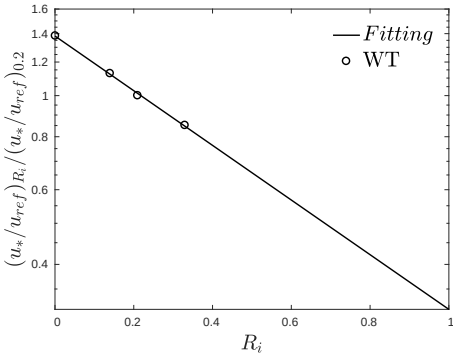

(a)

Figure 5: (a) The data of u_*/u_{ref} at $R_i = 0, 0.14, 0.21, 0.33$ in Marucci et al. (2018b) fitted to an exponential–function of R_i number, normalised by that at $R_i = 0.21$.

Marucci et al. (2018b) found that the ratio of turbulent stresses to the friction velocity (i.e. $\overline{u'u'}/u_*^2$) did not change significantly in the vicinity of the wall in various weakly stable conditions. We therefore assumed that this ratio was constant between $R_i = 1$ and $R_i = 0.21$. The turbulent stresses for '$R_i = 1^*$' at the inlet were determined from the estimated friction velocity u_* obtained from Fig 5. The estimated TKE prescribed at inlet for '$R_i = 1^*$' was about 10% of that for '$R_i = 0.21$'.

4. LES validation and verification

4.1. Validation

Predictions of turbulence, dispersion and mean temperature at $R_i = 0.21$ were validated against the wind tunnel (WT) data reported in Marucci et al. (2018b) and (Marucci & Carpentieri, 2018a). The standard error of the experimental measurements was around $\pm 1\%$ for mean velocity, $\pm 5\%$ for mean concentration and turbulent variances (Marucci et al., 2018b; Marucci & Carpentieri, 2018a). Mean velocity and temperature, streamwise and lateral turbulent stresses, mean concentration and concentration variance from the point source $S2$ were compared with wind tunnel data measured at $x = 16h$ and $z = 0$.

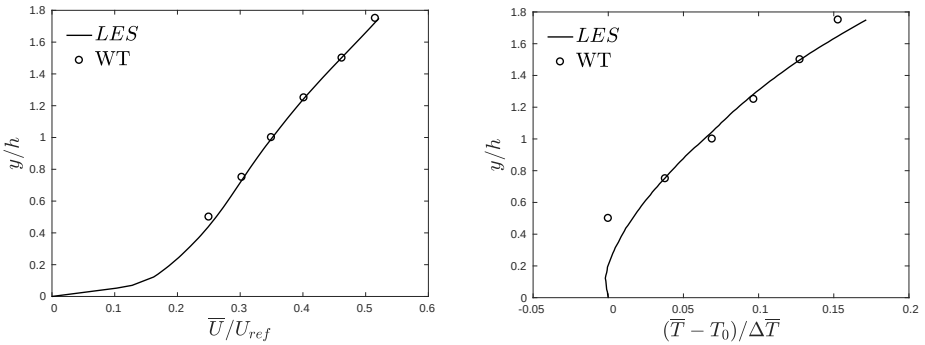

(a) (b)

Figure 6: (a) Vertical profiles of laterally averaged mean velocity from LES and experiments. (b) Vertical profiles of mean temperature from LES and wind tunnel (WT).

LES mean velocity (Fig. 6a) and mean temperature (Fig. 6b) were spatially averaged over four identical street intersections at $x = 16h$, whereas the experimental data were averaged in time only. The LES predictions of mean velocity were found to be in good agreement with experimental values below and immediately above the canopy(Fig. 6a). Similarly, the experimental profile of mean temperature was well captured by LES although the experimental uncertainty in temperature measurements close to the ground is not negligible.

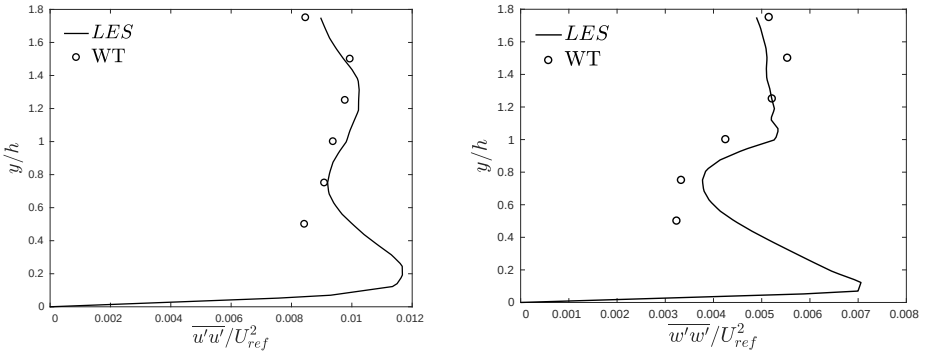

(a) (b)

Figure 7: (a) Vertical profiles of laterally averaged streamwise turbulent stress 6(a)and lateral turbulent stress 6(b) from LES and wind tunnel (WT).

Figure 7 presents comparisons between LES predictions of the mean streamwise and lateral turbulent stresses again averaged over four identical street intersections at $x = 16h$ with the corresponding experimental data. The small differences between the second–order statistics in the LES and wind tunnel data in the figures demonstrate the success of the validation. The differences may reasonably be attributed to comparing spatial averages from the LES with a single sampling station in the experimental data.

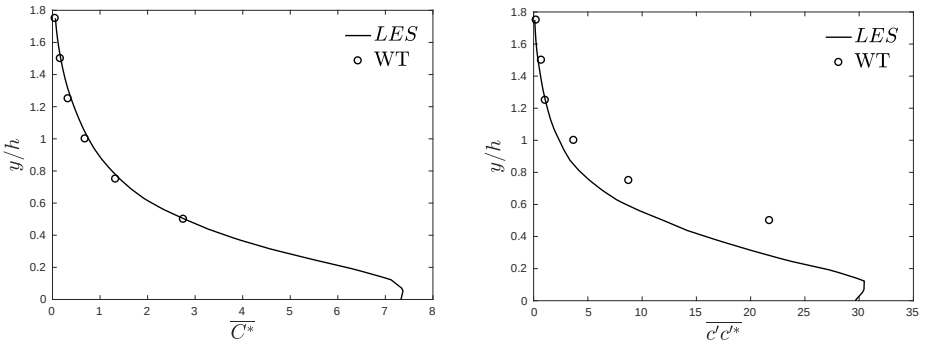

(a) (b)

Figure 8: (a) Vertical profiles of laterally averaged mean concentration (a) and vertical concentration variance (b) from LES and wind tunnel (WT).

The scalar concentration from the point source $S2$ was normalised following the method of Sessa et al. (2018) and Fuka et al. (2017):

$$\overline{C^*} = \overline{C}\frac{u_{ref}L_{ref}^2}{Q}, \tag{8}$$

where the characteristic length L_{ref} was the building height h and Q was the emission rate. Similarly, the scalar variance was normalized as:

$$\overline{c'c'^*} = \left[\frac{\sqrt{\overline{c'c'}}u_{ref}L_{ref}^2}{Q}\right]^2. \tag{9}$$

Laterally averaged LES mean concentration (Fig. 8a) and scalar variance (Fig. 8b) data were sampled at the main street intersection ($x = 16h$, $z = 0$) and compared with the experimental data. It can be seen that the LES accurately predicted the experimental mean concentration for $y \geq 0.5h$. The close agreement suggests that the predicted mean concentration at ground level should also be accurate. Figure 8b shows that the concentration variance was also well predicted above the canopy, but under-estimated within it. This difference may well be due to the uncertainties in measuring the concentration variance in the wind tunnel, and the source shape/size differences which affect the results in the near field (Sessa et al., 2018).

4.2. Ground temperature sensitivity test

As discussed in Sec. 3.3, Marucci et al. (2018b) used the least–square fitting method of Hancock & Hayden (2018) to obtain the upstream mean temperature profile and the temperature at the surface. From this they determined a good fit close to the ground. They then determined that the stability level in the wind tunnel was $R_i = 0.21$ by considering the maximum temperature difference $\Delta\overline{T} = 16K$ between the cooled floor $\overline{T_0}$ and the free stream flow $\overline{T}_{ref}$.

Although the temperature comparison was good, because of the experimental uncertainty in determining the surface temperature, the sensitivity of the derived value of R_i to this must be assessed. A ground surface temperature sensitivity assessment was therefore conducted to assess to what extent turbulence

and dispersion within and above the canopy were affected by a small change in ground temperature at the inlet. One case was simulated using the inlet mean temperature profile shown in Fig. 3a but changing the temperature profile in the vicinity of the ground (i.e. for $y \leq 0.125h$) to be a constant which was 2K lower than $\overline{T}_0$ in Section 4.1.

The normalised total heat flux, $\psi^{u_*}_{h,tot}$, in the direction of flow resulting from the prescribed inlet temperature profile (Fig. 3a) can be estimated.

$$\psi^{u_*}_{h,tot} = \int_{y/h \in (0,12)} \frac{(\overline{U}\,\overline{T} + \overline{u'T'})}{u_* T_*} d\left(\frac{y}{h}\right), \tag{10}$$

where u' and T' are the velocity and temperature fluctuations respectively. As discussed above, the temperature in the vicinity of the ground was changed between the two LES cases for $y \leq 0.125h$ only. This meant that the incoming heat flux was only expected to change below $y = 0.125h$. It is to be noted that close to the ground the turbulent flux component $\overline{u'T'}$ in Eq. 10 is always very small or negative compared to the advective part $\overline{U}\,\overline{T}$ (Fuka et al., 2017; Goulart et al., 2019). Similarly, the advective component $\overline{U}\,\overline{T}$ in the vicinity of the ground is also very small as the mean velocity is nearly zero.

Vertical profiles of mean velocity and turbulent stresses were sampled at $x = 16h$ and laterally averaged over 60 locations. The mean concentration from point source $S2$ was sampled in the lateral direction at $x = 16h$ and $y = 0.5h$ below the canopy, and normalized as in Eq. 8. As expected, the mean velocity, turbulent stresses and normalised concentration values for the two cases were found to be in close agreement. This confirmed that small differences in incoming heat flux due to the measurement errors in ground surface temperature had a negligible effect on the downstream turbulence and dispersion within and above the canopy.

4.3. Inlet TKE sensitivity test

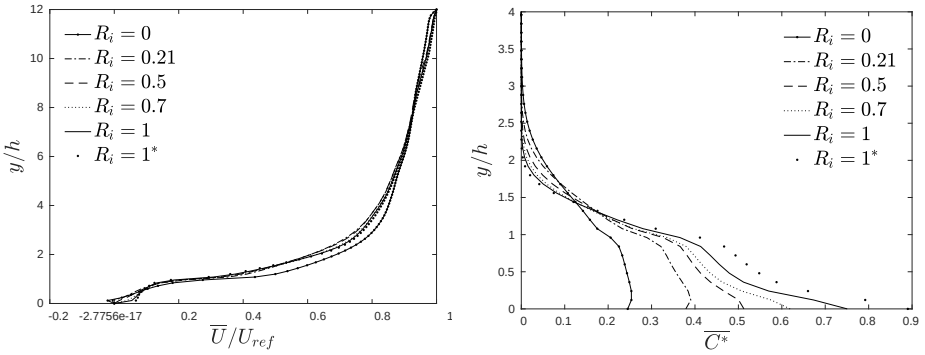

(a) (b)

Figure 9: Vertical profiles of mean velocity (a) and normalized concentration from the line source (b) measured at $x = 16h$ and laterally averaged over 60 locations.

Vertical profiles of mean velocity (Fig. 9a) and normalized mean concentration (Fig. 9b) were sampled at $x = 16h$ and laterally averaged over 60 locations. The effect of applying an inflow with a much lower TKE (i.e. '$R_i = 1^*$') on the mean velocity profile at $x = 16h$ was negligible. This shows that the difference between the mean velocity $x = 16h$ for $R_i = 0$ and the stable cases was mainly due to the small difference in the velocity profiles at the inlet (Fig. 4).

Figure 9b shows vertical profiles of laterally averaged mean concentration at $x = 16h$ for the line source $S1$ at various stratification levels. It is to be noted that dispersion from the line source is a quasi–$2D$ problem where the plume is laterally homogeneous. Increasing stability yielded higher concentrations within the canopy and lower concentrations above it. These effects were found to be further enhanced by prescribing much lower TKE at the inlet. The increase in concentration below the canopy also demonstrates the impact of reduced vertical mixing above it.

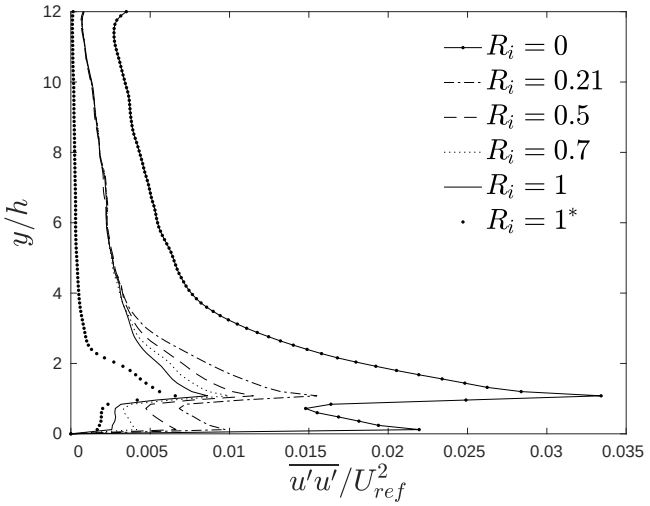

(a)

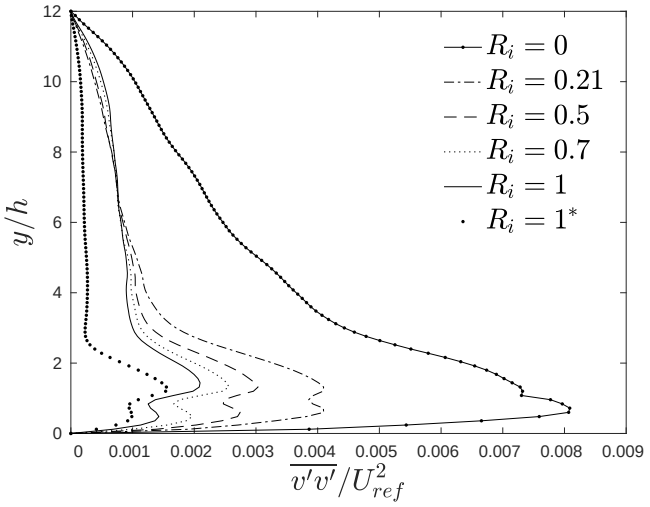

(b)

Figure 10: Vertical profiles of streamwise (a) and vertical (b) turbulent stresses laterally averaged over 60 points at $x = 16h$.

Figures 10a and 10b respectively show vertical profiles of streamwise and turbulent stresses laterally averaged over 60 points at $x = 16h$. The effects of inflow TKE and thermal stability are clearly visible one both quantities. For $R_i = 0.2, 0.5, 0.7, 1$, both the streamwise and the vertical stresses were found to

be reduced within and above the canopy by increasing stability. For the cases $R_i = 0.2, 0.5, 0.7, 1$, the differences above $\sim 6h$ were negligible due to the same inflow turbulence conditions being imposed at the inlet. On the contrary, for the cases $R_i = 0$ and '$R_i = 1^*$', the different turbulence conditions imposed at the inlet led to substantial differences in turbulent stresses at $x = 16h$ above the height $6h$ compared to the other cases. The evident differences in the $R_i = 0, 1$ and 1^* profiles demonstrate the importance of applying the correct inflow TKE for a chosen stability level.

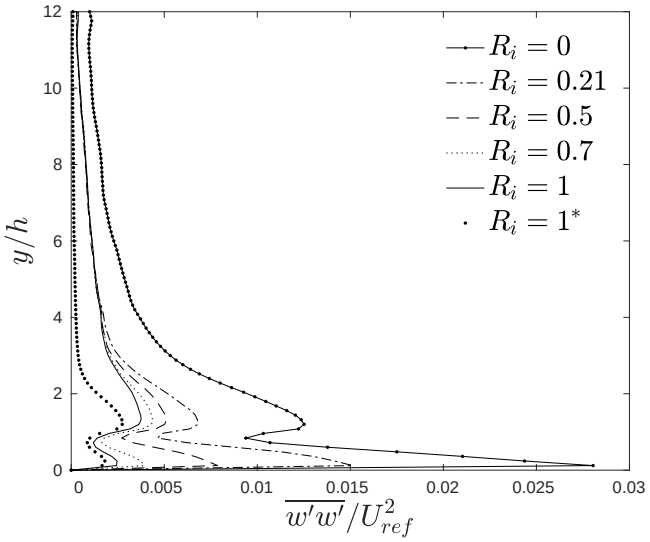

(a)

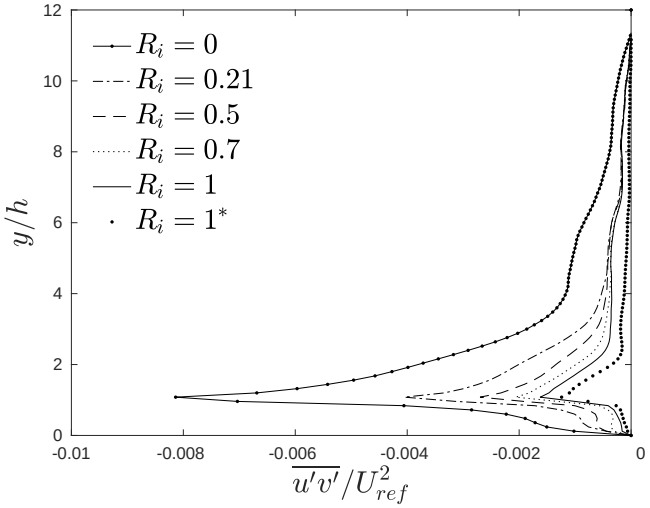

(b)

Figure 11: Vertical profiles of lateral normal turbulent stress (a) and shear stress (b) measured at $x = 16h$ and laterally averaged over 60 locations. Estimated TKE at inlet for '$R_i = 1^*$'.

Figure 11 shows laterally averaged vertical profiles of lateral normal turbulent stress and turbulent shear stress at $x = 16h$. Similarly to the profiles of streamwise and vertical turbulent stresses in Fig. 10, both the lateral normal

turbulent stress and turbulent shear stress profiles showed no visible differences above $\sim 6h$ for for $R_i = 0.2, 0.5, 0.7, 1$, while within and immediately above the canopy increasing stability damped the lateral normal turbulent stress and turbulent shear stress. For the '$R_i = 1^*$' case, both the turbulent stresses were lower than those for $R_i = 1$, due to the much lower TKE prescribed at the inlet, which was nearly zero above $4h$.

5. Stability effects on the internal boundary layer

The transition from the rough surface upstream of the array to the much higher roughness of the array itself causes an internal boundary layer IBL to develop from the leading edge of the array. In neutral stratification conditions, the IBL increases in depth as it develops downstream over the array and the flow within it has greater turbulent kinetic energy than that in the external boundary layer (e.g. Sessa et al., 2018). Given that IBLs develop at rural to urban transitions etc, and affect the dispersion in urban areas, it is important to understand their characteristics and how these affect the dispersion of pollutants at various stability levels.

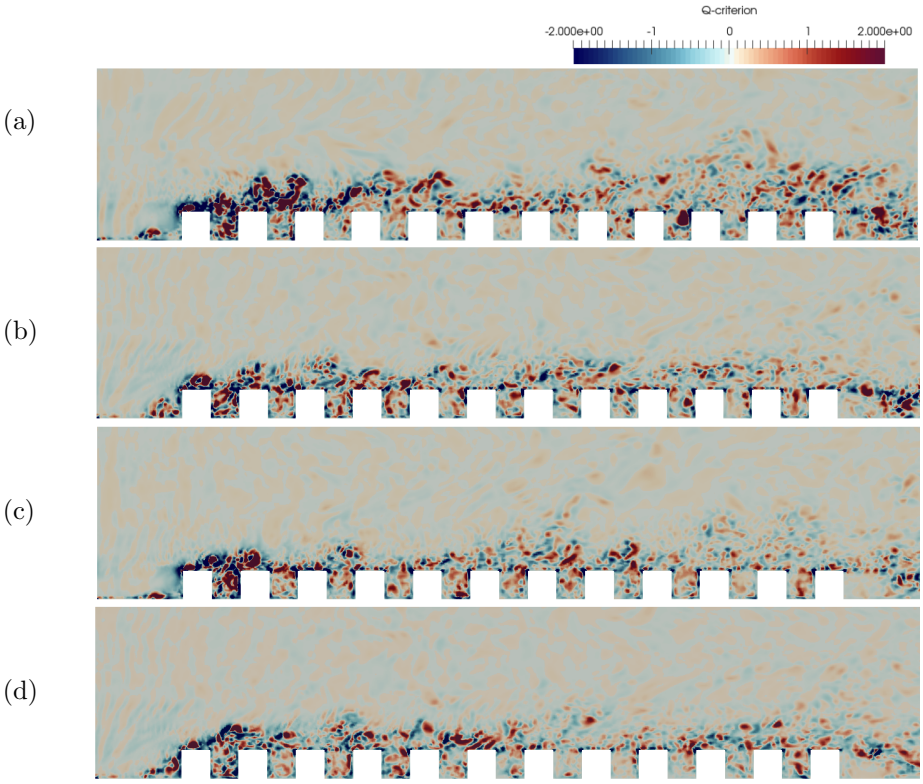

Figure 12: Q–criterion analysis of flow at $z = -1.5h$ for various stratification conditions and same inflow turbulence conditions. $R_i = 0.21$ (a), $R_i = 0.5$ (b), $R_i = 0.7$ (c), $R_i = 1$ (d).

The Q–criterion is defined as,

$$Q = 0.5(\Omega_{ij}\Omega_{ij} - S_{ij}S_{ij}), \tag{11}$$

where $\Omega_{ij} = 0.5(\frac{\partial u_i}{\partial x_j} - \frac{\partial u_j}{\partial x_i})$ and $S_{ij} = 0.5(\frac{\partial u_i}{\partial x_j} + \frac{\partial u_j}{\partial x_i})$. It is useful for highlighting flow regions in which rotation is dominant over the shear. Figure 12 shows the results of Q criterion analyses for $R_i = 0.2$ (Fig. 12a), $R_i = 0.5$ (Fig. 12b), $R_i = 0.7$ (Fig. 12c) and $R_i = 1$ (Fig. 12d) cases. The IBL was shallower and of a lower growth rate compared to weaker thermal stratification. The Q–criterion analyses were repeated for several cross-sections in the lateral direction with similar results.

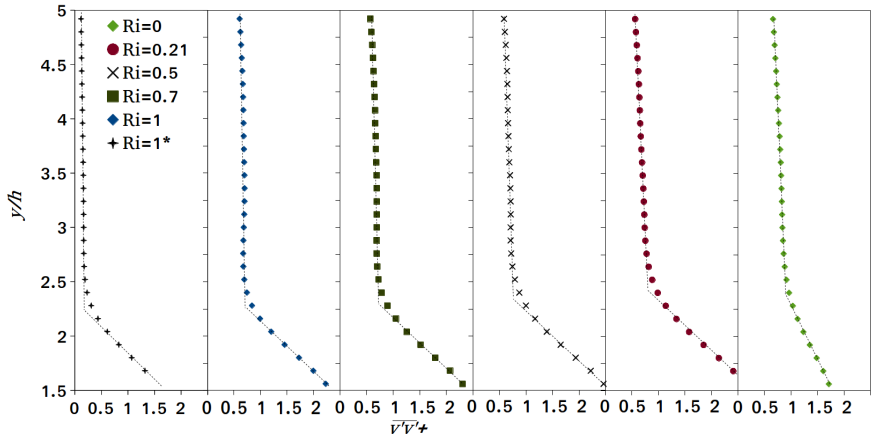
Ri=0
Ri=0.21
Ri=0.5
Ri=0.7
Ri=1
Ri=1*
y/h
5
4.5
4
3.5
3
2.5
2
1.5
0 0.5 1 1.5 2
$\overline{v'v'}+$

(a)

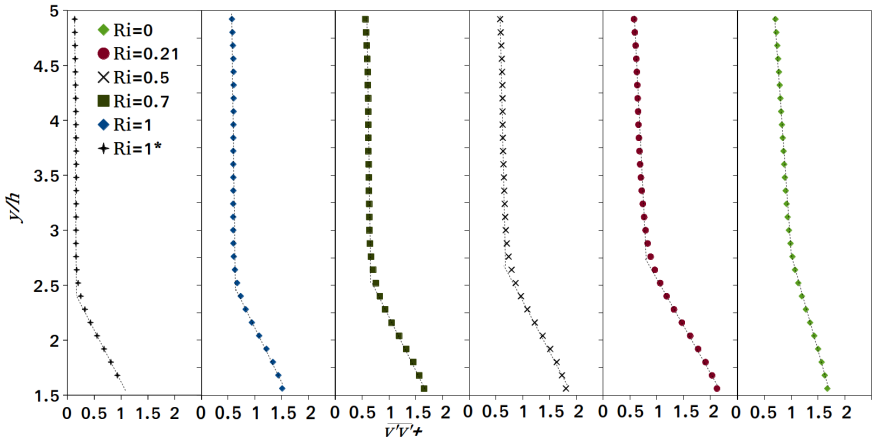
Ri=0
Ri=0.21
Ri=0.5
Ri=0.7
Ri=1
Ri=1*
y/h
5
4.5
4
3.5
3
2.5
2
1.5
0 0.5 1 1.5 2
$\overline{v'v'}+$

(b)

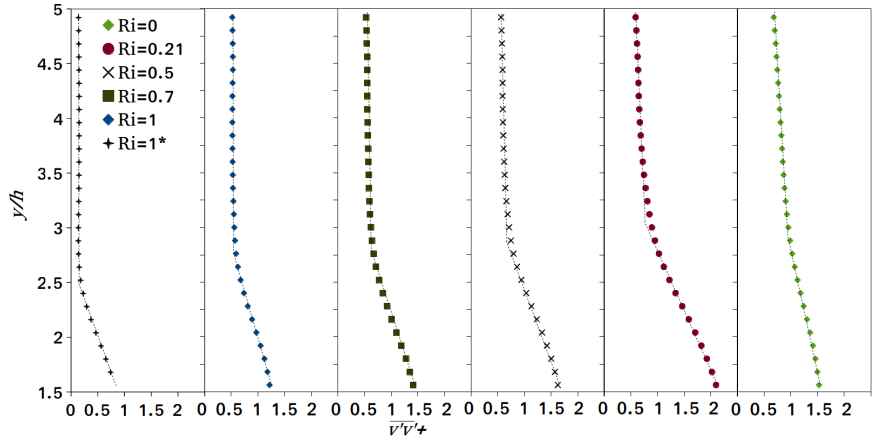

(c)

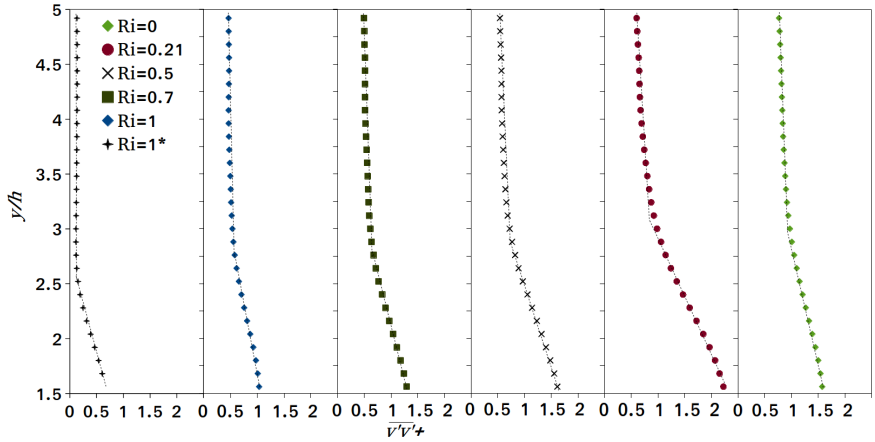

(d)

Figure 13: Vertical profiles of wall–normal turbulent stress $\overline{v'v'}^+$ at $x = 6h$ (a), $x = 10h$ (b), $x = 14h$ (c) and $x = 18h$ (d), averaged over 60 points in the lateral direction.

The method described in (Sessa et al., 2018) was used to process the data from each lateral street downstream of the leading edge of the array to locate the height of the IBL interface for various stability cases(Fig.13). This involves deriving vertical profiles above the canopy by laterally averaging the dimensionless wall–normal turbulent stress $\overline{v'v'}^+$, and is easy to implement and provides a reasonable indication of the IBL development. Figure 13 plots vertical profiles of wall–normal turbulent stress immediately above the canopy, shows visible

discontinuities in these profiles. Fitting linearly these profiles to two straight lines yieled intersections (i.e. "knee" points). These were identified as the interface of the internal and external boundary layer, which was consistent with the Q-criterion analyses shown in Fig. 12. This approach is in a similar manner to the methods of Antonia & Luxton (1972) and Efros & Krogstad (2011). The vertical stress profiles in the external and internal boundary layer regions were linearly fitted to a residual error of less than 2% in call cases.

Figure 13 shows that for the case '$R_i = 1^*$' the wall-normal turbulent stress was much smaller than the other cases because less TKE was prescribed at the inlet. On the contrary, for the $R_i = 0$ case, the wall–normal turbulent stress was greater than for the other stable cases because of the greater level of TKE defined at the inlet.

In Fig. 13a for $x = 6h$ the intersection of the two straight lines shows the height of the IBL interface was approximately the same for all the LES cases. This is due to a strong recirculation bubble formed at the leading edge, whose size was relatively insensitive to the inflow turbulence and thermal stability. At $x = 10h$ (Fig. 13b) and farther downstream $x = 14h$ and $18h$ (Figs. 13c and 13d), the effects of thermal stability on the depth of the IBL were more evident and the IBL was found to be shallower as the stratification was increased from $R_i = 0$ to $R_i = 1$. These results confirm that increasing the thermal stratification damped the turbulence and mixing, and led to a thinner IBL. It is to be noted that the local mean temperature gradient within the IBL is much greater than that above it (Fig. 3a), resulting in a greater local stratification effect on the turbulence and mixing in the IBL and almost a step-change in normal Reynolds stress at the interface.

Figures 13a – 13d show that under the same stratification, lower incoming turbulence (i.e. '$R_i = 1^*$') yields a shallower IBL compared to greater incoming turbulence (i.e. '$R_i = 1$'). This suggests that an approaching boundary layer with lower turbulence intensity is more susceptible to the effect of local thermal stratification over an urban area. This is consistent with the work of Williams et al. (2017) who found that the critical Richardson number for a rough wall was

greater than for a smooth wall. This also emphasises the importance of modelling the non-linear interaction between the incoming turbulence and locally generated turbulence in thermally stratified conditions.

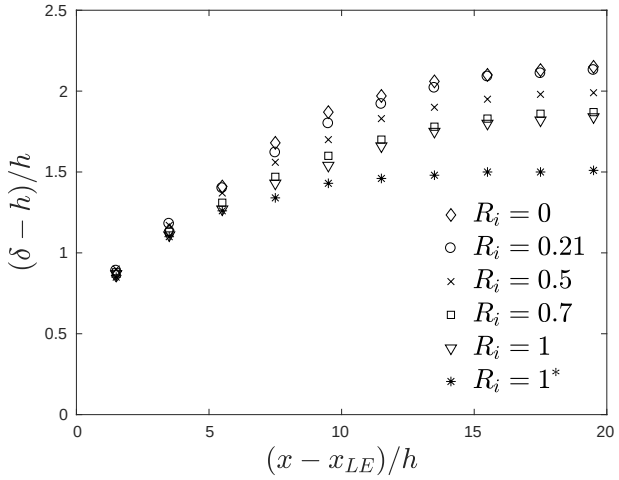

Figure 14: IBL height δ for different stratification conditions derived using the method of Sessa et al. (2018) based on vertical profiles of wall–normal turbulent stress $\overline{v'v'}^+$. x_{LE} is the streamwise coordinate of the leading edge of the array.

Figure 14 shows the IBL height δ for different stratification conditions derived by using the method of Sessa et al. (2018) based on vertical profiles of wall–normal turbulent stress $\overline{v'v'}^+$. It can be seen that the overall depth and growth rate of the IBL were sensitive to both the thermal stability and inflow turbulence conditions. Increasing stratification leads to a reduced IBL depth and a lower growth rate. A reduced TKE at the inlet ('$R_i = 1^*$') enhances these effects further compared to the case '$R_i = 1$'. The depth of the IBL varies by up to 30% within the studied range of thermal stratification conditions. Given that the present work has only considered weakly stably stratified conditions, we can conclude that both the depth of the IBL and the turbulence below and above it following a change in surface roughness are significantly affected by even small changes in thermal stratification.

6. Pollutant dispersion

The effects of stable stratification on pollutant dispersion were investigated by considering the emission of a passive scalar from a line source $S1$ (Fig. 1). This setup is useful for studying the effect of stratification on scalar concentration and scalar fluxes. As the periodic boundary conditions were used in the lateral direction, dispersion from the line source was a quasi–$2D$ problem because the scalar plume was laterally homogeneous.

6.1. Stability effects on scalar fluxes

The total vertical flux $\psi_{tot}^{v*} = \psi_{adv}^{v*} + \psi_{turb}^{v*}$ includes contributions from both advective (Eq. 12) and turbulent (Eq. 13) scalar fluxes. The advective and turbulent vertical concentration fluxes transport pollutants from the canopy flow to the boundary layer above. The dimensionless advective and turbulent vertical flux components are defined respectively as follows (Fuka et al., 2017):

$$\psi_{adv}^{v*} = \overline{V}\,\overline{C}\frac{h^2}{Q} \tag{12}$$

$$\psi_{turb}^{v*} = \overline{v'c'^*} = (\overline{VC} - \overline{V}\,\overline{C})\frac{h^2}{Q} \tag{13}$$

where v' and c' are the vertical velocity and concentration fluctuations respectively and $\overline{V}$ is the mean vertical velocity.

Similarly, the total streamwise flux in the streamwise direction is defined as follows:

$$\psi_{tot}^{u*} = (\overline{U}\,\overline{C} + \overline{u'c'})\frac{h^2}{Q} \tag{14}$$

where u' is the streamwise velocity fluctuation and $\overline{U}$ is the mean streamwise velocity.

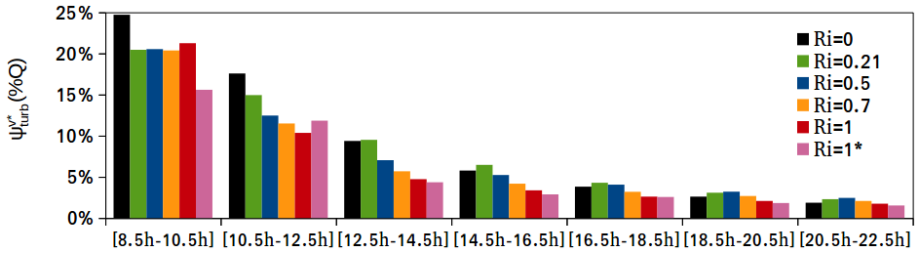

Figure 15: Integrated turbulent vertical concentration flux for horizontal planes $2h \times 12h$ at $y = 1h$ at 7 streamwise locations for various stratification conditions. Line source placed at $x = 10h$.

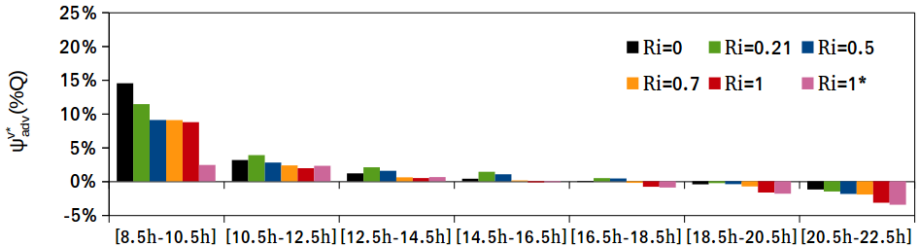

Figure 16: Integrated advective vertical concentration flux for horizontal planes $2h \times 12h$ at $y = 1h$ at 7 streamwise locations for various stratification conditions. Line source placed at $x = 10h$.

The vertical turbulent (Fig. 15) and advective (Fig. 16) concentration fluxes from the line source $S1$ were integrated at the canopy height $y = 1h$ across the entire span $12h$, between two x coordinates separated by $2h$.

$$\psi^{a,b} = \int \int_{x/h \in (a,b), y/h=1} \psi^{v*} d\left(\frac{x}{h}\right) d\left(\frac{z}{h}\right). \tag{15}$$

Large positive turbulent and advective fluxes were found over the first interval ($x = 8.5h - 10.5h$) because the horizontal plane was above the source street ($x = 10h$). Further downstream, the turbulent and advective concentration flux components decreased significantly. Figures 15 and 16 show that the turbulent flux was generally greater in magnitude than the advective flux.

Both the turbulent and the advective fluxes generally decreased as R_i was increased from 0.2 to 1.0, given the same turbulent inflow conditions. This confirmed that increasing stratification reduced vertical transport of pollutant

due to decreasing both the turbulent and advective scalar fluxes in the vertical direction. For $R_i = 0$, because of higher TKE prescribed at inlet, the general pattern was slightly different. For example, at the third downstream interval from the line source ($x = 14.5h - 16.5h$), the turbulent scalar flux (Fig. 15) was found to be lower than that for $R_i = 0.2$. This was due to higher turbulent kinetic energy near the source which yielded greater vertical transport above the canopies than that for $R_i = 0.2$. For '$R_i = 1^*$', the much lower TKE at the inlet caused significantly low turbulent and advective scalar fluxes over the source street ($x = 8.5h - 10.5h$). As a result, the scalar plume for '$R_i = 1^*$' was strongly advected into the following lateral street ($x = 10.5h - 12.5h$), producing a so–called virtual secondary source. Figures 15–16 show that over the first two lateral streets both the turbulent and advective scalar fluxes for '$R_i = 1^*$' have almost the same magnitude. This again confirms the existence of the virtual secondary source in the 2^{nd} street.

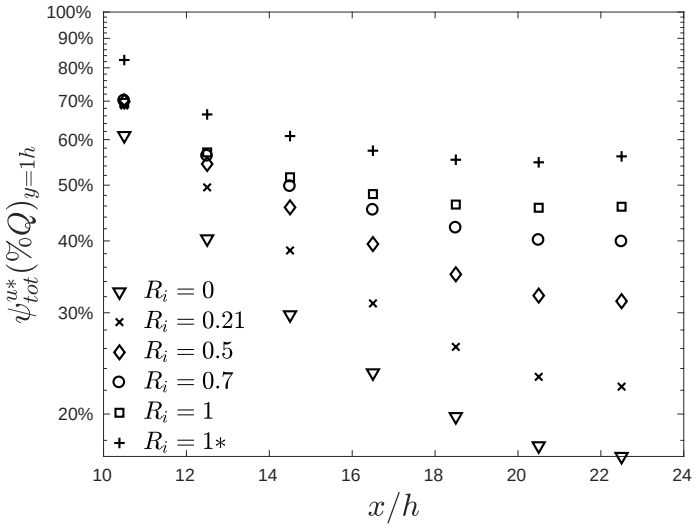

(a)

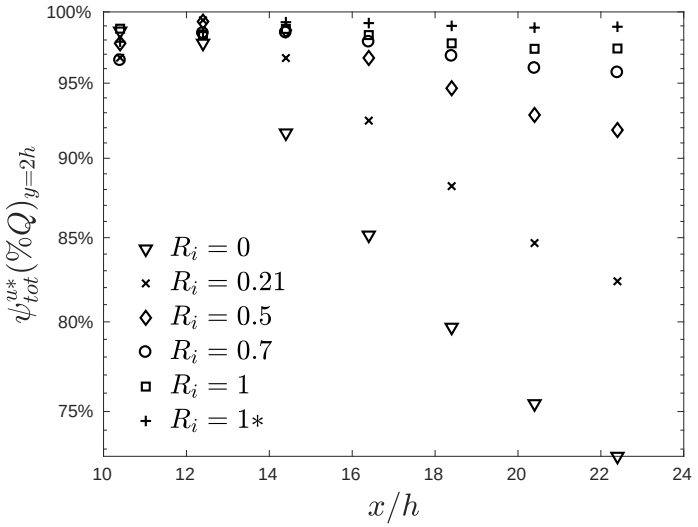

(b)

Figure 17: Total streamwise flux over $1h \times 12h$ (a) and $2h \times 12h$ (b) vertical planes at 7 streamwise locations downstream of the line source (at $x = 10h$).

The streamwise total concentration flux (Eq. 14) of the line source $S1$ was integrated over vertical planes with dimensions ($1h \times 12h$) as shown in Fig. 17a and ($2h \times 12h$) as shown in Fig. 17b. The integration was performed between

two constant y coordinates across the entire span. For example, at $x = 10.5h$, the total flux was computed as follows:

$$\psi^{a,b} = \int\int_{y/h\in(a,b),x/h=10.5} \psi^{u*} d\left(\frac{y}{h}\right) d\left(\frac{z}{h}\right). \tag{16}$$

Figure 17a shows the amount of pollutant transported in the streamwise direction below the canopy top. Near the line source, approximately 60% of the total emission Q for $R_i = 0$ was transported in the streamwise direction while $\sim$ 40% of the emission Q was transported vertically through the horizontal plane above the source street. Further downstream, the amount of pollutant transported in the streamwise direction dropped to less than 20% of the total flux for $x \geq 20h$.

From $R_i = 0.2$ to $R_i = 1$ a similar amount of pollutant was transported downstream at $x = 10.5h$ because the kinetic energy close to the source was similar in all cases. Away from the source, greater stability trapped more pollutant within the canopy layer. In the range $R_i = 0.2$ to $R_i = 1$ the total concentration flux below the canopy increased by more than 50% at $x/h = 20$ which is 5 rows of bocks downstream from the line source. For the case '$R_i = 1^*$' with lower incoming TKE, the stratification effect is evidently stronger compared to the case $R_i = 1$.

Figure 17b shows the amount of pollutant transported through the vertical plane below $y = 2h$ in the streamwise direction. All of the profiles show a peak value at approximately $x = 12.5h$. The vertical plane at $x = 10.5h$ was very close to the line source at $x = 10h$, where the gradient of total streamwise flux, and consequently the error in integrated total streamwise flux through the plane was greatest. This might explain why the integrated total streamwise flux at $x = 10.5h$ shown in Fig. 17b is not 100%. Further downstream, the total streamwise flux through the vertical plane $y = 0 - 2h$ increases monotonically as the stratification level increases for the same incoming turbulence intensity, confirming again that the spreading of the plume is evidently affected by the stability level. Furthermore, reducing incoming turbulence resulted in an in-

crease in total streamwise flux through the vertical plane $y = 0 - 2h$ at the same stratification.

6.2. Stability effects on mean concentration

As stated earlier in Section 6, within the LES simulations the dispersion from a ground–level constant line source can be considered to be laterally homogeneous, with spreading of the plume constrained in the lateral direction. The previous sections show that increasing R_i decreased the vertical scalar transport above the canopy and led to higher concentrations close to the ground. In this section, we quantify these effects on mean concentration.

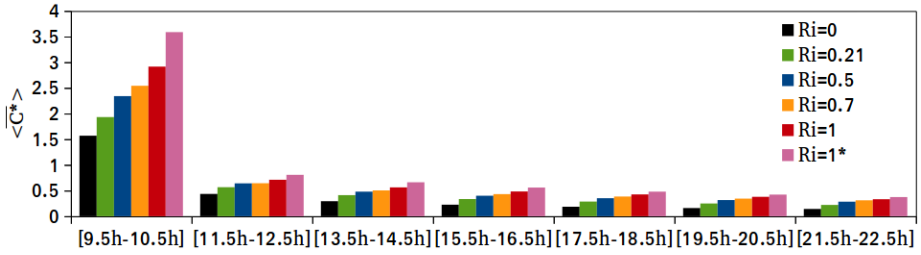

Figure 18: Volume–average of normalized mean concentration within lateral streets, from the ground to the canopy height $y = 1h$. The lateral source street is defined at $x = 9.5 - 10.5h$.

The volume–averaged concentration was calculated within each lateral street up to the canopy height, starting from the source street which was located between $x = 9.5h$ and $x = 10.5h$. Mean concentration from the line source $S1$ was normalized as in accordance with Eq. 8 and averaged over a volume with dimensions $1h \times 1h \times 12h$:

$$< \overline{C^*} >^{a,b} = \int_{x/h\in(a,b)} \int_{y/h\in(0,1)} \int_{z/h\in(-6,6)} \overline{C^*} d\left(\frac{x}{h}\right) d\left(\frac{y}{h}\right) d\left(\frac{z}{h}\right). \quad (17)$$

Figure 18 shows that the volume–averaged concentration increased monotonically in all of the streets as the thermal stability was increased, and decreased with distance from the source at all stratification conditions. This is because increased stability suppresses turbulence resulting in reduced vertical mixing within and above the canopy (see Fig.13). Figure 18 also shows that

the volume–averaged concentration was increased when a lower TKE was prescribed at the inlet in the case '$R_i = 1^*$' compared to that in the case $R_i = 1$. This is consistent with a reduction in vertical scalar flux in the case '$R_i = 1^*$' compared to that in the case $R_i = 1$ (Sec. 6.1).

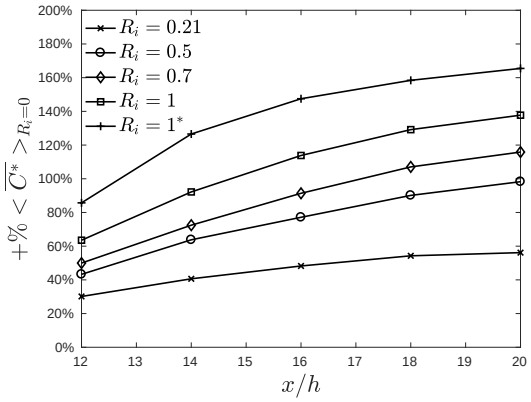

Figure 19: Increase (%) in volume–averaged concentration $< \overline{C^*} >$ for cases at $R_i \geq 0.2$ compared to $R_i = 0$ within lateral streets up to the canopy height.

Figure 19 shows a monotonic increase in volume–averaged concentration within each lateral street for cases at $R_i \geq 0.2$ compared to that within the same street for case $R_i = 0$. This again confirms the effect of increasing thermal stratification and the lower TKE in the approaching flow for the $R_i = 1^*$ case shows a 20% increase in volume–averaged concentration.

7. Conclusions and discussion

In this paper we have rigorously examined the effects of various levels of weakly stable stratification ($0 \leq R_i \leq 1$) on turbulence and dispersion over a rural–to–urban transition region using a high–fidelity large eddy simulation (LES) approach. Firstly we validated the LES predictions against wind tunnel measurements on a stratified boundary layer approaching a regular array of cuboid elements at $R_i = 0.21$. The validation suggested that our developed synthetic inflow generation method embedded in LES was able to accurately

predict mean velocities, turbulent stresses, mean concentration and variance of concentration fluctuations from a ground–level point source in weakly stratified flows over a rough–to–very–rough transition region, such as from rural–to–urban region. It is to be noted that this is the first time we carried out assessment of synthetic generation of turbulence and temperature fluctuations for modelling a developing weakly stable atmospheric boundary layer.

A numerical sensitivity test was conducted to assess whether a small change of ground temperature upstream of the step change in roughness affected turbulence and dispersion further downstream. This was required to assess the potential impact of the non–negligible errors of measuring the ground temperature upstream of the step change in the experiments. We found that the differences in incoming heat flux due to changes in the surface temperature were negligible because the mean streamwise velocity was nearly zero in the vicinity of the ground. We conclude that the turbulence and dispersion downstream of the step change in roughness was insensitive to small changes of ground temperature upstream of the step change.

The transition from a rough surface to a much rougher surface composed of an array of regular cuboids generated an internal boundary layer (IBL) from the leading edge of the array. The method developed in Sessa et al. (2018) was used to evaluate the depth of the IBL for the different stratification conditions simulated (i.e. $0 \leq R_i \leq 1$) and different inflow turbulence intensities. We found that the IBL became shallower as the thermal stratification was increased. The greater local vertical temperature gradient within the IBL than in the external boundary layer led to a greater local stratification effect within the IBL and consequently a more pronounced step-change of normal Reynolds stress at the the interface of IBL.

We also found that the IBL height was reduced as the level of TKE was reduced in the approaching flow for the same stratification condition. This suggests that an approaching boundary layer with less turbulence intensity is more susceptible to the effect of local thermal stratification over an urban area. This also suggests the importance of accurately modelling the non-linear inter-

action between the incoming turbulence and the locally generated turbulence in thermal stratification conditions.

The dispersion and scalar fluxes from a ground–level line source placed behind the fifth row of elements downstream of the leading edge were analysed extensively in various stratification conditions ($0 \leq R_i \leq 1$). The total vertical flux decreased above the lateral streets whereas the horizontal total flux increased within the lateral streets as the thermal stratification was increased. This led to larger volume-averaged concentrations within streets with increasing stratification. If the TKE in the approaching boundary layer is reduced while maintaining the same level of thermal stratification, the effect on the total scalar fluxes within and above the canopy, and on the volume-averaged mean concentration within lateral streets is greater.

We conclude that even weakly stable stratification ($0 \leq R_i \leq 1$) in an approaching boundary layer significantly changes the concentration levels that result from material dispersing from point or line sources within an array of blocks. This is because of the suppression of the turbulence in the IBL, and the reduced vertical transport of pollutant above the canopy.

Acknowledgements. VS is grateful to the Defence Science and Technology Laboratory and the University of Southampton for the funding of his PhD studentship. We thank to the EnFlo team at the University of Surrey for providing the wind tunnel data through the appropriate publications. We are also grateful to Prof Ian P. Castro, Dr Glyn Thomas and Mr Timothy Foat for helpful comments. The relevant data are available from the University of Southampton database, under the DOI (to be provided).

References

Antonia, R. A., & Luxton, R. E. (1972). The response of a turbulent boundary layer to a step change in surface roughness. part 2. rough-to-smooth. *Journal of Fluid Mechanics*, *53*, 737–757. doi:10.1017/S002211207200045X.

Bercin, K. M., Xie, Z.-T., & Turnock, S. R. (2018). Exploration of digital-filter and forward-stepwise synthetic turbulence generators and an improvement for their skewness-kurtosis. *Computers & Fluids*, *172*, 443 – 466. doi:https://doi.org/10.1016/j.compfluid.2018.03.070.

Boppana, V. B. L., Xie, Z. T., & Castro, I. P. (2013). Large-eddy simulation of heat transfer from a single cube mounted on a very rough wall. *Boundary-Layer Meteorology*, *147*, 347–368. doi:10.1007/s10546-012-9793-7.

Boppana, V. B. L., Xie, Z.-T., & Castro, I. P. (2014). Thermal stratification effects on flow over a generic urban canopy. *Boundary-Layer Meteorology*, *153*, 141–162. doi:10.1007/s10546-014-9935-1.

Britter, R. E., & Hanna, S. R. (2003). Flow and dispersion in urban areas. *Annual Review of Fluid Mechanics*, *35*, 469–496. doi:10.1146/annurev.fluid.35.101101.161147.

Castro, I. P., Xie, Z. T., Fuka, V., Robins, A. G., Carpentieri, M., Hayden, P., Hertwig, D., & Coceal, O. (2017). Measurements and computations of flow in an urban street system. *Boundary-Layer Meteorology*, *162*, 207–230. doi:10.1007/s10546-016-0200-7.

Cheng, H., & Castro, I. P. (2002). Near-wall flow development after a step change in surface roughness. *Boundary-Layer Meteorology*, *105*, 411–432. doi:10.1023/A:1020355306788.

Cheng, W., & Liu, C.-H. (2011). Large-eddy simulation of turbulent transports in urban street canyons in different thermal stabilities. *Journal of Wind Engineering and Industrial Aerodynamics*, *99*, 434 – 442. doi:https://doi.org/10.1016/j.jweia.2010.12.009. The Fifth International Symposium on Computational Wind Engineering.

Efros, V., & Krogstad, P.-A. (2011). Development of a turbulent boundary layer after a step from smooth to rough surface. *Experiments in Fluids*, *51*, 1563–1575. doi:10.1007/s00348-011-1167-2.

Fuka, V., Xie, Z. T., Castro, I. P., Hayden, P., Carpentieri, M., & Robins, A. G. (2017). Scalar fluxes near a tall building in an aligned array of rectangular buildings. *Boundary-Layer Meteorology*, . doi:10.1007/s10546-017-0308-4.

Goulart, E., Reis, N., Lavor, V., Castro, I., Santos, J., & Xie, Z. (2019). Local and non-local effects of building arrangements on pollutant fluxes within the urban canopy. *Building and Environment*, *147*, 23 – 34. doi:https://doi.org/10.1016/j.buildenv.2018.09.023.

Hancock, P. E., & Hayden, P. (2018). Wind-tunnel simulation of weakly and moderately stable atmospheric boundary layers. *Boundary-Layer Meteorology*, *168*, 29–57. doi:10.1007/s10546-018-0337-7.

Hanson, R. E., & Ganapathisubramani, B. (2016). Development of turbulent boundary layers past a step change in wall roughness. *Journal of Fluid Mechanics*, *795*, 494–523. doi:10.1017/jfm.2016.213.

Hertwig, A., Soulhac, L., Fuka, V., Auerswald, T., Carpentieri, M., Hayden, P., Robins, A., Xie, Z., & O, C. (2018). Evaluation of fast atmospheric dispersion models in a regular street network. *Environ. Fluid Mech.*, *18*, 1007–1044.

Inagaki, M., Kondoh, T., & Nagano, Y. (2005). A mixed-time-scale sgs model with fixed model-parameters for practical LES. *Journal of Fluids Engineering*, *127*, 1–13. doi:10.1115/1.1852479.

Kanda, I., & Yamao, Y. (2016). Passive scalar diffusion in and above urban-like roughness under weakly stable and unstable thermal stratification conditions. *Journal of Wind Engineering and Industrial Aerodynamics*, *148*, 18–33. doi:10.1016/j.jweia.2015.11.002.

Marucci, D., & Carpentieri, M. (2018a). Wind tunnel study on the effect of atmospheric stratification on flow and dispersion in an array of buildings, . ICUC10: 10th International Conference on Urban Climate, 6 10 August, 2018, New York, USA.

Marucci, D., Carpentieri, M., & Hayden, P. (2018b). On the simulation of thick non-neutral boundary layers for urban studies in a wind tunnel. *International Journal of Heat and Fluid Flow*, *72*, 37 – 51. doi:https://doi.org/10.1016/j.ijheatfluidflow.2018.05.012.

Ohya, Y. (2001). Wind-tunnel study of atmospheric stable boundary layers over a rough surface. *Boundary-Layer Meteorology*, *98*, 57–82. doi:10.1023/A:1018767829067.

Okaze, T., & Mochida, A. (2017). Cholesky decompositionbased generation of artificial inflow turbulence including scalar fluctuation. *Computers & Fluids*, *159*, 23 – 32.

Sessa, V., Xie, Z.-T., & Herring, S. (2018). Turbulence and dispersion below and above the interface of the internal and the external boundary layers. *Journal of Wind Engineering and Industrial Aerodynamics*, *182*, 189 – 201. doi:https://doi.org/10.1016/j.jweia.2018.09.021.

Tomas, J. M., Pourquie, M. J. B. M., & Jonker, H. J. J. (2016). Stable stratification effects on flow and pollutant dispersion in boundary layers entering a generic urban environment. *Boundary-Layer Meteorology*, *159*, 221–239. doi:10.1007/s10546-015-0124-7.

Williams, O., Hohman, T., Van Buren, T., Bou-Zeid, E., & Smits, A. J. (2017). The effect of stable thermal stratification on turbulent boundary layer statistics. *Journal of Fluid Mechanics*, *812*, 10391075. doi:10.1017/jfm.2016.781.

Wood, C. R., Lacser, A., Barlow, J. F., Padhra, A., Belcher, S. E., Nemitz, E., Helfter, C., Famulari, D., & Grimmond, C. S. B. (2010). Turbulent flow at 190 m height above london during 2006–2008: A climatology and the applicability of similarity theory. *Boundary-Layer Meteorology*, *137*, 77–96. doi:10.1007/s10546-010-9516-x.

Xie, Z. T., & Castro, I. P. (2008). Efficient generation of inflow conditions for

large eddy simulation of street-scale flows. *Flow, Turbulence and Combustion*, *81*, 449–470. doi:10.1007/s10494-008-9151-5.

Xie, Z.-T., Hayden, P., & Wood, C. R. (2013). Large-eddy simulation of approaching-flow stratification on dispersion over arrays of buildings. *Atmospheric Environment*, *71*, 64 – 74. doi:http://dx.doi.org/10.1016/j.atmosenv.2013.01.054.

Yassin, M., Kato, S., Ooka, R., Takahashi, T., & Kouno, R. (2005). Field and wind-tunnel study of pollutant dispersion in a built-up area under various meteorological conditions. *Journal of Wind Engineering and Industrial Aerodynamics*, *93*, 361 – 382. doi:https://doi.org/10.1016/j.jweia.2005.02.005.